Deep learning algorithms rely on digital pathology to classify tissue tumors, where the whole tissue slides are digitized and imaged. The produced multi-resolution whole slide images (MWSIs) are with high resolution that may range from about 100,000 to 200,000 pixels. MWSIs are often stored in a multi-resolution configuration to simplify the processing of images, navigation, and efficient exposition. This work develops a network for classifying MWSIs that require high memory employing a deep neural Inception-v3 architecture. This work employs the MWSIs from Camelyon16, which is around 451 GB in size of Challenge dataset from two independent sources including 400 MWSIs as a total of lymph nodes. The training dataset contains 111 MWSIs of tumor tissue and lymph nodes and 159 WSIs of normal lymph nodes. The developed model uses sample-based processing to train extensive MWSIs employing the MATLAB platform. The model introduces transfer learning techniques with an Inception-v3-based architecture to categorize separate samples as a tumor or normal. Therefore, the main aim here is to achieve two-classes binary segmentation containing normal and tumor. This includes creating a new fully connected layer for the Inception-v3 architecture with two classes and compensating new layers instead of the original final fully-connected layers. The results obtained demonstrated that the heatmap visualization can recognize the boundary coordinates of ground truth as sketchy Region Of Interest (ROI), where the green boundary represents the normal regions and the tumor area with red boundaries. The proposed Inception v3 Convolutional Neural Network (CNN) architecture can achieve more than 92.8 % accuracy for such MWSIs dataset to categorize brain tumors into normal and tumor tissue

Keywords: convolutional neural network, deep learning, classification, Inception architecture, brain tumor

UDC 621
DOI: 10.15587/1729-4061.2023.281227

DEVELOPING A CONVOLUTIONAL NEURAL NETWORK FOR CLASSIFYING TUMOR IMAGES USING INCEPTION V3

Ali A. Mahmood
Master of Computer Science, Information Technology*
Sadeer Sadeq
Master of Computer Engineering*
Yaser Issam Aljanabi
Master of Computer Engineering-Artificial Intelligence
Turkiye/Ankara
Department of Computer Engineering
Ministry of Higher Education and Scientific Research/
Minister Office
College of Electrical and Electronic Engineering Techniques
Middle Technical University
Zafaraniyah, Baghdad, Iraq, 10074
Ahmad H. Sabry
Corresponding author
Doctor of Control and Automation Engineering
Department of Computer Engineering
Al-Nahrain University
Al Jadriyah Bridge, Baghdad, Iraq, 64074
E-mail: ahs4771384@gmail.com
*Head Office
University of Information Technology and Communications
Al-Mansour, Baghdad, Iraq, 10013

Received date 08.04.2023
Accepted date 18.06.2023
Published date 30.06.2023

How to Cite: *Mahmood, A. A., Sadeq, S., Aljanabi, Y. I., Sabry, A. H. (2023). Developing a convolutional neural network for classifying tumor images using inception V3. Eastern-European Journal of Enterprise Technologies, 3 (9 (123)), 86–93. doi: https://doi.org/10.15587/1729-4061.2023.281227*

1. Introduction

After cardiovascular disorders, cancer is the second biggest cause of death. Brain cancer has the lowest survival rate of any type of cancer. Several forms of brain tumors exist depending on the location, shape, and texture of the tumor. A precise tumor-type diagnosis enables the doctor to select the best course of action and even save the patient's life. A Computer Aided Diagnosis (CAD) system to aid physicians and radiologists in the detection and classification of cancers is desperately needed in the field of artificial intelligence. Deep learning has demonstrated promising performance in computer vision systems in recent years [1, 2]. A dangerous condition, brain tumors are responsible for a rising number of fatalities. Magnetic resonance imaging (MRI)-based manual tumor diagnosis takes a lot of time and is ineffective for precisely identifying, locating, and classifying the type of tumor [3]. There are several complexities in the categorization of brain tumors by magnetic resonance imaging (MRIs); first, the high-density nature of the brain makes some difficulties to classify brain tumors; and second, the intertwining of tissues in brain structure and the difficulty of it [4]. Developed differential deep-CNN architecture has the advantage of analyzing the image pattern and pixel direction by means of contrast computations and its capability to categorize a huge dataset without technical problems and with high accuracy [4, 5].

Patients' chances of survival can be increased by early detection and treatment of liver cancer. The most comprehensive information for the differential diagnosis of liver

cancers comes from dynamic contrast-enhanced MRI. Yet, as MRI diagnosis is influenced by personal experience, deep learning might offer a fresh approach to diagnosis [6]. In the past several years, academics have focused a lot of attention on Deep Learning, the newest and most popular trend in the field of machine learning. Deep learning has been widely employed in multiple applications as a powerful machine learning method for handling various complicated problems that call for exceptionally high accuracy and sensitivity, particularly in the medical industry. In general, brain tumors are among the most prevalent and severe malignant tumor disorders, and if they are identified at a higher stage, they might result in a very short predicted life. Thus, grading a brain tumor is a very important step to take after finding the tumor in order to develop a successful treatment strategy [7].

In the area of medical image analysis, classifying brain tumors is a challenging task. Radiologists may quickly and readily identify the tumor without requiring surgery thanks to evolving algorithms and machine learning technology [4]. Deep learning algorithms have made great strides in the processing and analysis of medical images in recent years. However, there are numerous challenges associated with identifying brain cancers using magnetic resonance imaging, including the complexity of the brain's structure and the interconnection of its tissues, as well as the challenge of diagnosing brain tumors given the great density of the brain. Therefore, research is devoted to the development of an effective deep learning model for classifying such high-resolution images of tumors and that is relevant.

2. Literature review and problem statement

Several studies compared a number of deep learning methods and classical machine learning methods for classifying tumor images of lymph nodes. The study [8] covered four traditional machine-learning techniques: random forests, support vector machines, adaptive boosting, and artificial neural networks. 1,397 lymph nodes taken from 168 individuals' PET/CT scans were used to evaluate the methodologies, and the findings of the accompanying pathology examination served as the gold standard. The assessment was conducted by means of 10 times cross-validation according to Area Under the Curve (AUC), accuracy (ACC), specificity, and the criterion of sensitivity. The convolutional Neural Network (CNN), human doctors from our institute, and conventional approaches were contrasted using the best feature set. The findings showed that the diagnostic characteristics produced considerably higher AUC and ACC values (0.870.92 and 8,185 %, respectively) than texture features. Specificity, sensitivity, AUC, and ACC for CNN were 0.91, 86, 88, and 84, respectively. However, tumor identification from magnetic resonance images (MRIs) becomes a time intense method and is inadequate for precisely classifying, localizing, and detecting tumor type.

The paper [3] also addressed brain tumor classification localization and detection with a multi-model two-phase automatic analysis. The model contained preprocessing, feature classification by the support vector machine (SVM) with an error-correcting output codes approach, and feature extraction by a CNN. The paper classified the MRIs into abnormal and normal images to detect brain tumors using region-based CNN (VGG-19, Visual Geometry Group (VGG)-16, and AlexNet). Although the results of this work demonstrated that 99.55 % was achieved for 349 images as maximum detection accuracy, the dataset of the study was with a limited image resolution of lymph nodes tumor.

The study [9] proposed a CNN model that included two parts: learning algorithms and architecture to optimize the network training parameters. The authors reported accuracy results for the enhancing regions, core, and complete as 0.84, 0.85, and 0.90 respectively for the dataset (BRATS 2016 brain tumor). Although all the pixels of an MR image are classified and attained a good performance, the segmentation accuracy was not sufficient to be generalized on other larger datasets. CNN deep learning architecture to classify the brain tumors of a weighted contrast-enhanced brain MR dataset of 3,064 T1 images into Pituitary Tumor, Meningioma, and Glioma was proposed by the study [7]. The study obtained a sensitivity of 98.18 % and an accuracy of 98.93 % for the picked lesions, 98.52 % sensitivity, and 99 % accuracy for the uncropped lesions. However, the obtained application was not valid over a larger dataset.

Based on CNN classification for the histologic patterns on surgical resection slides, a lung adenocarcinoma classifier was proposed by [10]. The CNN model identifies regions of neoplastic cells, then collects the classifier to minor histologic patterns and infers predominant and for every specified image from 143 whole-slide datasets. The study's approach may be valid for any whole-slide image classifications, but the classification accuracy was limited. This limitation also includes the Artificial Intelligence (AI-based) method proposed by [11]. In the same context, the study [6] developed a CNN model of a deep learning system for classifying liver tumor images according to laboratory test results and clinical data including text, unenhanced MR images, and enhanced MR images. The results demonstrated that deep learning CNN can achieve high-performance accuracy. This approach required very clean images for the processed dataset. A good evaluation model has been presented in the study [1], where the proposed model is performed over a dataset including 3 brain tumor types (Pituitary tumors, Gliomas, and Meningiomas) of 3,064 MRI images. However, this architecture was very complicated and requires long time and parameter settings.

All aforementioned literature allows us to assert that it is expedient to conduct a study on the use of a deep learning network to classify normal and tumor tissues by creating a new fully connected layer with two classes and compensating new layers instead of the original final fully-connected layers to help early detection of brain tumors.

3. The aim and objectives of the study

The aim of the study is to achieve two-classes binary segmentation containing normal and tumor. This includes creating a new fully connected layer for the Inception-v3 architecture with two classes and compensating new layers instead of the original final fully-connected layers. This will make it possible to process the MWSIs dataset and help early detection of brain tumors.

To achieve this aim, the following objectives are accomplished:

– to calculate and visualize the heatmap for the test images for indicating the ROI boundary coordinates (tumor and normal regions) of ground truth;

– to obtain a confusion matrix and consequently get the accuracy of classification;

– to compare the classification results with the ground truth ROI boundary coordinates;

– to quantify the developed architecture estimation.

4. Method and materials

4. 1. Object and research hypothesis

The main objective is to classify multi-resolution whole slide images (MWSIs) that require high memory by using a deep neural Inception-v3 architecture. The developed model uses sample-based processing to train extensive MWSIs employing the MATLAB platform and its function of the deep learning tools. The model introduces transfer learning techniques with an Inception-v3-based architecture to categorize separate samples as a tumor or normal. The model architecture of the developed deep learning Inception-v3 is shown in Fig. 1.

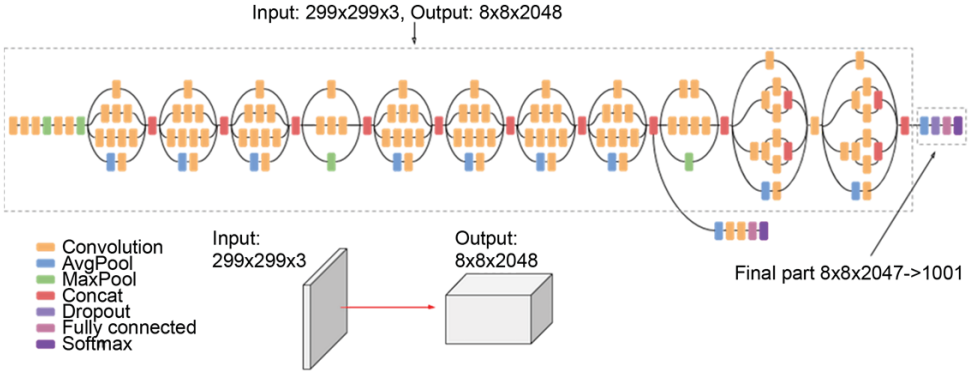

Fig. 1. Inception v3 architecture [12]

Therefore, two classes of binary segmentation containing normal and tumor must be achieved ultimately. This includes creating a new fully connected layer for the Inception-v3 architecture with two classes and compensating new layers instead of the original final fully-connected layers.

4. 2. Dataset

This work employs the multi-resolution whole slide images (MWSIs) from Camelyon16 [13], which is around 451 GB in size of Challenge dataset from two independent sources including 400 WSIs as a total of lymph nodes. The Camelyon16 test image dataset contains 130 MWSIs including both tumor and normal tissue with approximately 2 GB size each. This data divides the images into 270 for training and 130 for testing. The MWSIs are saved in an 11-level pyramid structure of a stripped format and TIF files. The training dataset contains 111 WSIs of tumor tissue and lymph nodes and 159 WSIs of normal lymph nodes. The tumor images are accompanied by ground truth coordinates of the lesion boundaries. The data set is around 451 GB in size.

4. 3. Training Inception-v3 Network

This work employs deep Inception V3 network [14], which is a convolutional neural network architecture in transfer learning trained with an Image-Net dataset [15]. The network includes 48 deep layers for classifying more than a million images into 1,000 object categories such as animals, trees, buildings, etc. The deep Inception V3 network has learned a wide range of rich feature representations of images of input size 299×299. The image features are extracted by the network convolutional layers, while the final classification layer and the last learnable layer classify input images based on image features. The two final layers provide class information probabilities by combining the image features, predicted labels, and loss values. The names of these two final layers are "*ClassificationLayer_predictions*" and "*predictions*". This work retrains a pre-trained architecture for classifying new images by replacing these two final layers with layers modified to agree on the tumor medical images. The flowchart demonstrating preparing of data, setting up the Inception V3 architecture, and identifying training options is shown in Fig. 2.

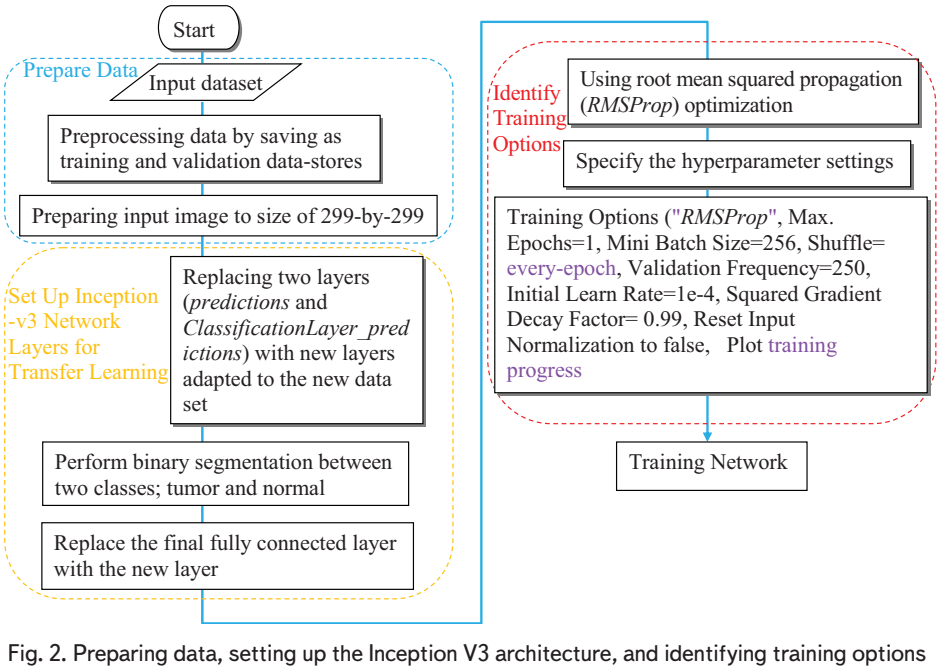

Fig. 2. Preparing data, setting up the Inception V3 architecture, and identifying training options

As described in the flowchart, the Inception V3 architecture was modified by creating the required classification layer of the two categories and replacing the last categorization layer with a new layer to fit the input image features. The hyperparameter optimization settings of root mean squared propagation (RMSProp) [16] have been used to train the developed network. The maximum epochs have been reduced to a small value since the large training data facilitates to achieve convergence faster. The minimum batch size is set according to GPU memory availability, where a large min. patch size enables us to accomplish the training earlier. However, larger min. patch size can decrease the capability of the architecture to cover general modes. A false is set to the (ResetInputNormalization) parameter for preventing the normalization stats computation when a full read of the training data is performed. This work also used a modified pre-trained network to suit the input images to save the time of network training.

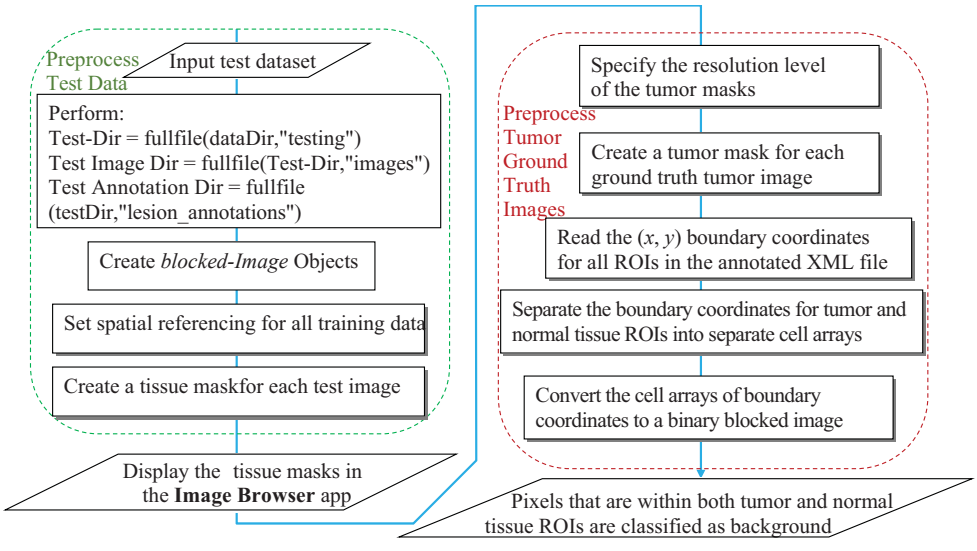

Fig. 3. Flowchart showing the preprocessing of test data and preprocessing of tumor ground truth images

4. 4. Pre-processing data

The pre-processing data includes downloading the test dataset, specifying a directory for the test images, and creating blocked Image Objects for Managing the Test Image dataset. Every blocked Image object refers to its correspondence file on memory. Then, the spatial referencing from the TIF file metadata is set for the whole training dataset. In this stage, it is possible to produce tissue masks. To process the MWSI dataset proficiently, a tissue mask is created for every test image. This method is identical to the one applied in the training preprocessing of normal images. This work set the normal Mask-Level to 8 and 512*512 block sizes. Each tissue mask has only one level and is small sufficient to fit in a disk. In this stage, we show samples of tissue masks, Fig. 3.

The second stage of this diagram is the Image pre-processing Ground Truth of Tumor data, where specifying the level of image resolution for the tumor mask data is performed with a tumor Mask-Level equal to (8). For each tumor image ground truth, we create a tumor mask following the steps:

– for every region of interest (ROI), we read the boundary (x, y) coordinates in the interpreted XML folder;

– for normal and tumor tissue ROI images, we divide the boundary coordinates into disconnected cell arrays;

– exchanging to a binary blocked image for the boundary coordinate cell arrays, where the background refers to normal tissue pixels and the ROI of binary images refers to tumor pixels. ROIs Pixels that are within both normal and tumor tissue are categorized as background.

4. 5. Heatmaps Prediction for Tumor Possibility

The heatmap can give a probability indication for every block whether there is a tumor category. To calculate the heatmap for every test image, this work uses the trained categorization architecture. We perform the following functions over every test image to obtain the heatmap:

– selecting all blocks that include one tissue pixel minimum through computing an argument called (theta), which represents the Inclusion Threshold;

– processing blocks' batches by applying a (predict-Block) function, which returns the probable score of there is a tumor in the block after contacts each prediction block of data;

– writing the heatmap files to a TIF folder, where the last outcome after handling the whole blocks is a heatmap demonstrating the potential of encountering tumors through the full MWSI;

– heatmap Visualization.

4. 6. Classifying of testing images

In order to classify the blocks of testing images into normal and tumor, an application of specific thresholding is performed over all the heatmap probability scores. The blocks are categorized as a tumor when the value of tumor probability is above the threshold (0.8). In an ideal world, the calculation of this level of threshold depends on the precision-recall curves or the ROC (Receiver Operating Characteristic) over the validation dataset. A flowchart demonstrates the processing stages of heatmaps prediction of tumor probability, classifying test images at a particular threshold, classification results, and quantifying the network prediction is shown in Fig. 4.

The classification of the blocks for all test images and calculation of the confusion matrix are performed using the following processes on every heatmap image:

– applying a threshold on each heatmap image;

– to match the heatmap size, we perform resizing and refining the ground truth mask;

– for the entire blocks, we compute the confusion matrix at the optimum resolution point;

– saving the confusion matrix components (FN, TN, FP, and TP) in a blocked image as a structure;

– saving the classification predictions as numerically labeled images in blocked images, where FN, TN, FP, and TP results are represented by the values 0, 1, 2, and 3, respectively;

– over the entire test image, we compute the global confusion matrix;

– confusion matrix visualization;

– classification Result Visualizing is implemented by comparing the classification results with the ROI boundary coordinates of ground truth;

– based on computing the area under the curve AUC-ROC curve, we quantify the network prediction at various threshold values [1 0.9 0.99:.1:–.1 0 0.05];

– using the trapezoidal concept, we also compute the AUC metric, which is in the range of (0–1).

Fig. 5. Samples of the created tissue masks from the dataset

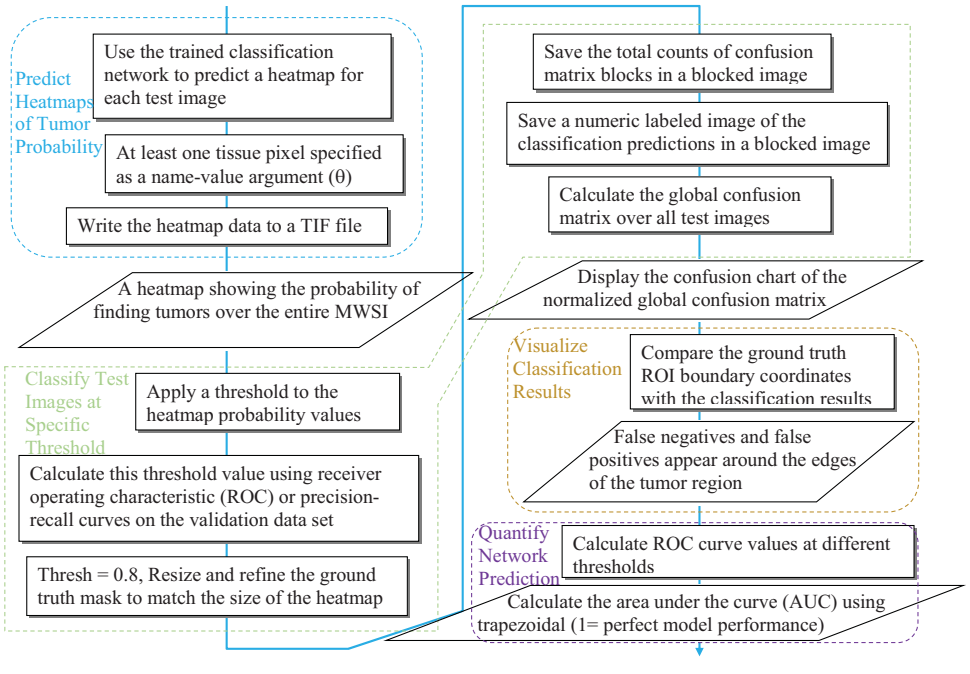

Fig. 4. The processing stages of heatmaps prediction of tumor probability, classifying test images at a particular threshold, classification results, and quantifying the network prediction

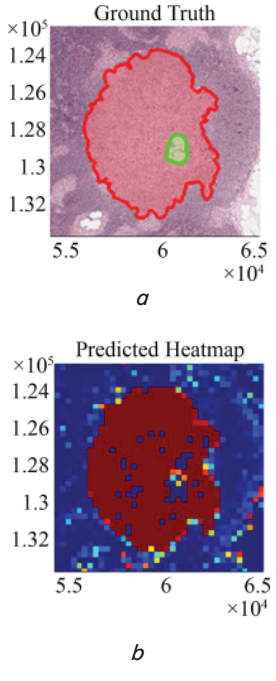

Fig. 6. Heatmap visualization of one sample from the dataset: *a* – ground truth; *b* – prediction heatmap

5. Results of classifying tumor images using Inception v3

5. 1. The Heatmap Visualization

This work set the normal Mask-Level to 8 and 512×512 block sizes. Each tissue mask has only one level and is small sufficient to fit in a disk. Fig. 5 shows samples of the created tissue masks from the dataset.

These samples indicate that the stage for preprocessing of test data and preprocessing of tumor ground truth images is ready. To calculate the heatmap for every test image, this work uses the trained categorization architecture. The last outcome after handling the whole blocks is a heatmap demonstrating the potential of encountering tumors through the full MWSI, one sample from the dataset is shown in Fig. 6.

The Heatmap Visualization includes selecting test images to put on view. The left-hand side part displays the boundary coordinates of ground truth as sketchy ROI. The green boundary, which represents the normal regions, can take place within tumor areas that are demonstrated by red boundaries. The right part of the figure shows the test image heatmap, where the ROI is extracted and zoomed in.

5. 2. Confusion matrix

The confusion matrix visualization is depicted in Fig. 7.

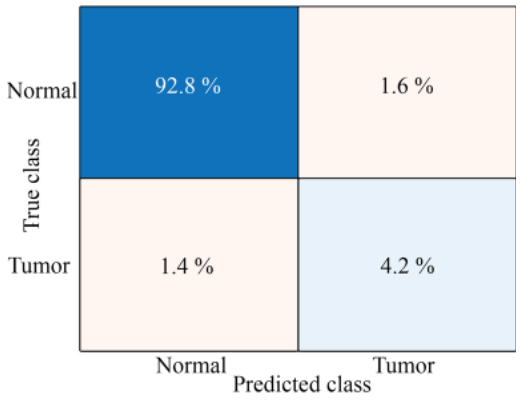

Fig. 7. The confusion matrix for the tested data

The confusion matrix lists the number of classification predictions that were false negative (FN), true nega-

tive (TN), false positive (FP), and true positive (TP). From the normalized global confusion matrix's confusion chart, it is found that because the normal tissue makes up the majority of the blocks in the MWSI images, there are many true negative predictions.

5. 3. Comparing the classification results with the ground truth Region Of Interest boundary coordinates

The comparison results of the classification obtained from the fusion matrix analysis with the ground truth ROI boundary coordinates for the same tumor sample are shown in Fig. 8.

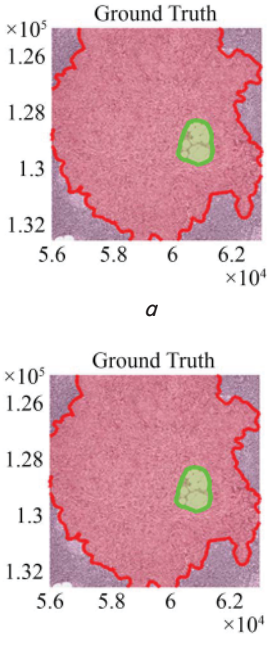

Fig. 8. The comparison between the classifications of fusion matrix analysis with the ground truth Region Of Interest boundary coordinates: *a* — ground truth; *b* — classified blocks

The result shows the border coordinates ground truth as sketchy ROIs on the left-hand side, while the right-hand side depicts the test image. In addition, an application of block-based coloring is performed on the confusion matrix.

5. 4. Quantifying Network estimation

According to computing the area under the curve (AUC) curve, we quantify the network prediction at various threshold values [1 0.9 0.99:.1:–.1 0 0.05]. Using the trapezoidal concept, we also compute the AUC metric, which is in the range (0–1). The AUC for the true positive rate with respect to the false positive rate is shown in Fig. 9.

A comparison with recent studies discussing tumor classification in different areas using machine learning architectures can be listed in a comparison table (Table 1).

It is found that the AUC is around 1 for this dataset, which represents the approaching to ideal performance for the developed network. For best results, the AUC can be employed to control the tuning in the training stage.

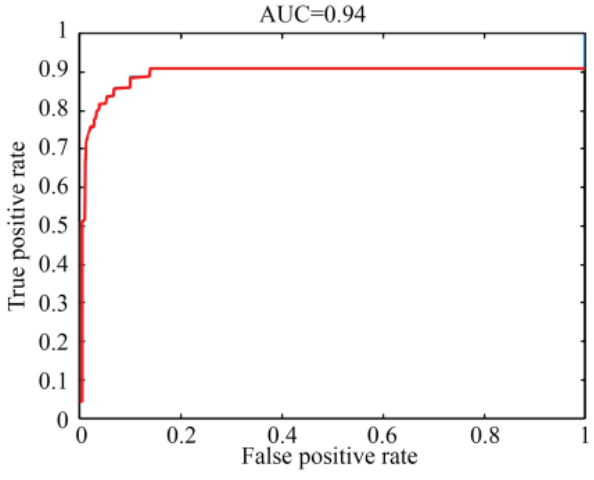

Fig. 9. Area under the curve for the true positive rate with respect to the false positive rate

Table 1

Comparison between the developed method and recent studies discussing tumor classification in different areas using machine learning architectures

References	Image type	Developed network	Application	Dataset	Achieved accuracy
[17]	Cystoscopicimages	U-Net CNN	Tumor bladder lesions	PubMed-MEDLINE database	90 %
[4]	25,000 MRIs	differential deep-CNN	Brain tumors	Not clear	90.25 %
[18]	Automated Breast Ultrasound (ABUS) images	Shared Extracting Feature Network (SEF-Net)	Breast tumor	Not clear	92.86 %
[19]	MRI	transfer deep-learning	Brain tumors	Not clear	90.75 %
[20]	Mammographic Image	U-Net CNN	Brain tumors	322 raw (MIAS) and 580 from Private datasets	91.7 %
[21]	MRI	Xception, CNN with ADAM optimizer	Brain tumors	Not clear	91.67 %
[22]	MRI	U-Net CNN	Brain tumor	MICCAI BraTS 2017	Not clear
This	MWSIs	Inception v3 CNN	Brain tumor	Camelyon16	92.8 %

6. Discussion of the results of classifying tumor images using Inception v3

A sample of the created tissue masks from the dataset was shown in Fig. 5, which indicates that the stage for preprocessing of test data and preprocessing of tumor ground truth images is ready for further analysis. We use the trained categorization architecture to calculate the heatmap for every test image. The last outcome after handling the whole blocks is a heatmap demonstrating the potential of encountering tumors through the full MWSI, one sample from the dataset was shown in Fig. 6. The left-hand side part of

heatmap visualization displays the boundary coordinates of ground truth as sketchy ROI. The green boundary, which represents the normal regions, can take place within tumor areas that are demonstrated by red boundaries. The right part of Fig. 6 shows the test image heatmap, where the ROI is extracted and zoomed in. The classification predictions have been saved as numerically labeled images in blocked images, where FN, TN, FP, and TP results are represented by the values 0, 1, 2, and 3, respectively. Over the entire test image, we computed the global confusion matrix. The classification result was implemented by comparing the classification results with the ROI boundary coordinates of ground truth. From the normalized global confusion matrix's confusion chart, it is found that because the normal tissue makes up the majority of the blocks in the MWSI images, there are many true negative predictions. Fig. 8 compared between the classifications of fusion matrix analysis with the ground truth ROI boundary coordinates. The result shows the border coordinates ground truth as sketchy ROIs on the left-hand side, while the right-hand side depicts the test image. In addition, an application of block-based coloring is performed on the confusion matrix.

False positives and false negatives occur at the borders of the tumor area, which indicates that the architecture has difficulty identifying blocks with fractional classes. The result shows true negatives with no color, false negatives as yellow, false positives as cyan and true positives as red. To decrease the error of classification in the area surrounding the tumor ROI, less homogenous blocks were used to retrain the network as shown in Fig. 9.

From a comparison between the developed method and recent studies such as the studies [17, 22] that used Cystoscopic images with U-Net CNN, and the study [19] that used MRI images with transfer deep learning, the developed Inception-v3 architecture achieved better accuracy. Furthermore, it is found that the AUC for the true positive rate with respect to the false positive rate is around 1 for the dataset considered in this study (Table 1). This represents the approaching to ideal performance for the developed network.

The proposed algorithm has been applied to this type of dataset, which may be considered as an applicability limitation, which can be improved to obtain the best results by employing the AUC to control the tuning in the training stage. A potential development might be considered when applying another type of dataset to expand the applicability of the proposed method.

The limitation of this approach is that it has been only applied to the Camelyon16 dataset, which is multi-resolution whole slide images (MWSIs). This can be taken into account as future work when expanding the application to more types of MWSI datasets.

7. Conclusions

1. The heatmap for the test images to indicate the ROI boundary coordinates (tumor and normal regions) of ground truth has been calculated and visualized to recognize between the tumor and normal tissue.

2. The achieved accuracy of tumor classification obtained from the confusion matrix was more than 92.8 % for such a huge MWSIs dataset.

3. The comparison of the classification results with the ground truth ROI boundary coordinates successfully categorizes between normal and tumor regions.

4. It is found that the AUC is around 1 for this dataset, which represents the approaching to ideal performance for the developed network.

Conflict of interest

The authors declare that they have no conflict of interest in relation to this research, whether financial, personal, authorship or otherwise, that could affect the research and its results presented in this paper.

Financing

The study was performed without financial support.

Data availability

Data will be made available on reasonable request.

References

1. Abdelaziz Ismael, S. A., Mohammed, A., Hefny, H. (2020). An enhanced deep learning approach for brain cancer MRI images classification using residual networks. Artificial Intelligence in Medicine, 102, 101779. doi: https://doi.org/10.1016/j.artmed.2019.101779
2. Sfayyih, A. H., Sabry, A. H., Jameel, S. M., Sulaiman, N., Raafat, S. M., Humaidi, A. J., Kubaiaisi, Y. M. A. (2023). Acoustic-Based Deep Learning Architectures for Lung Disease Diagnosis: A Comprehensive Overview. Diagnostics, 13 (10), 1748. doi: https://doi.org/10.3390/diagnostics13101748
3. Abd-Ellah, M. K., Awad, A. I., Khalaf, A. A. M., Hamed, H. F. A. (2018). Two-phase multi-model automatic brain tumour diagnosis system from magnetic resonance images using convolutional neural networks. EURASIP Journal on Image and Video Processing, 2018 (1). doi: https://doi.org/10.1186/s13640-018-0332-4
4. Abd El Kader, I., Xu, G., Shuai, Z., Saminu, S., Javaid, I., Salim Ahmad, I. (2021). Differential Deep Convolutional Neural Network Model for Brain Tumor Classification. Brain Sciences, 11 (3), 352. doi: https://doi.org/10.3390/brainsci11030352
5. Houssein, E. H., Emam, M. M., Ali, A. A., Suganthan, P. N. (2021). Deep and machine learning techniques for medical imaging-based breast cancer: A comprehensive review. Expert Systems with Applications, 167, 114161. doi: https://doi.org/10.1016/j.eswa.2020.114161
6. Zhen, S., Cheng, M., Tao, Y., Wang, Y., Juengpanich, S., Jiang, Z. et al. (2020). Deep Learning for Accurate Diagnosis of Liver Tumor Based on Magnetic Resonance Imaging and Clinical Data. Frontiers in Oncology, 10. doi: https://doi.org/10.3389/fonc.2020.00680

7. Alqudah, A. M. (2019). Brain Tumor Classification Using Deep Learning Technique - A Comparison between Cropped, Uncropped, and Segmented Lesion Images with Different Sizes. International Journal of Advanced Trends in Computer Science and Engineering, 8 (6), 3684–3691. doi: https://doi.org/10.30534/ijatcse/2019/155862019
8. Wang, H., Zhou, Z., Li, Y., Chen, Z., Lu, P., Wang, W. et al. (2017). Comparison of machine learning methods for classifying mediastinal lymph node metastasis of non-small cell lung cancer from 18F-FDG PET/CT images. EJNMMI Research, 7 (1). doi: https://doi.org/10.1186/s13550-017-0260-9
9. Hoseini, F., Shahbahrami, A., Bayat, P. (2018). An Efficient Implementation of Deep Convolutional Neural Networks for MRI Segmentation. Journal of Digital Imaging, 31 (5), 738–747. doi: https://doi.org/10.1007/s10278-018-0062-2
10. Wei, J. W., Tafe, L. J., Linnik, Y. A., Vaickus, L. J., Tomita, N., Hassanpour, S. (2019). Pathologist-level classification of histologic patterns on resected lung adenocarcinoma slides with deep neural networks. Scientific Reports, 9 (1). doi: https://doi.org/10.1038/s41598-019-40041-7
11. Mehrotra, R., Ansari, M. A., Agrawal, R., Anand, R. S. (2020). A Transfer Learning approach for AI-based classification of brain tumors. Machine Learning with Applications, 2, 100003. doi: https://doi.org/10.1016/j.mlwa.2020.100003
12. Advanced Guide to Inception v3. Cloud TPU. Google Cloud. Available at: https://cloud.google.com/tpu/docs/inception-v3-advanced
13. Litjens, G., Bandi, P., Ehteshami Bejnordi, B., Geessink, O., Balkenhol, M., Bult, P. et al. (2018). 1399 H&E-stained sentinel lymph node sections of breast cancer patients: the CAMELYON dataset. GigaScience, 7 (6). doi: https://doi.org/10.1093/gigascience/giy065
14. Szegedy, C., Vanhoucke, V., Ioffe, S., Shlens, J., Wojna, Z. (2016). Rethinking the Inception Architecture for Computer Vision. 2016 IEEE Conference on Computer Vision and Pattern Recognition (CVPR). doi: https://doi.org/10.1109/cvpr.2016.308
15. ImageNet. Available at:https://www.image-net.org/
16. Raharjo, B., Farida, N., Subekti, P., Herlina, S., Doddy, H., Rahim, R. (2021). Optimization forecasting using back-propagation algorithm. Journal of Applied Engineering Science, 19 (4), 1083–1089. doi: https://doi.org/10.5937/jaes0-30175
17. Negassi, M., Suarez-Ibarrola, R., Hein, S., Miernik, A., Reiterer, A. (2020). Application of artificial neural networks for automated analysis of cystoscopic images: a review of the current status and future prospects. World Journal of Urology, 38 (10), 2349–2358. doi: https://doi.org/10.1007/s00345-019-03059-0
18. Zhuang, Z., Ding, W., Zhuang, S., Joseph Raj, A. N., Wang, J., Zhou, W., Wei, C. (2021). Tumor classification in automated breast ultrasound (ABUS) based on a modified extracting feature network. Computerized Medical Imaging and Graphics, 90, 101925. doi: https://doi.org/10.1016/j.compmedimag.2021.101925
19. Alanazi, M. F., Ali, M. U., Hussain, S. J., Zafar, A., Mohatram, M., Irfan, M., AlRuwaili, R. et al. (2022). Brain Tumor/Mass Classification Framework Using Magnetic-Resonance-Imaging-Based Isolated and Developed Transfer Deep-Learning Model. Sensors, 22 (1), 372. doi: https://doi.org/10.3390/s22010372
20. Mahmood, T., Li, J., Pei, Y., Akhtar, F., Rehman, M. U., Wasti, S. H. (2022). Breast lesions classifications of mammographic images using a deep convolutional neural network-based approach. PLOS ONE, 17 (1), e0263126. doi: https://doi.org/10.1371/journal.pone.0263126
21. Asif, S., Yi, W., Ain, Q. U., Hou, J., Yi, T., Si, J. (2022). Improving Effectiveness of Different Deep Transfer Learning-Based Models for Detecting Brain Tumors From MR Images. IEEE Access, 10, 34716–34730. doi: https://doi.org/10.1109/access.2022.3153306
22. Jwaid, W. M., Al-Husseini, Z. S. M., Sabry, A. H. (2021). Development of brain tumor segmentation of magnetic resonance imaging (MRI) using U-Net deep learning. Eastern-European Journal of Enterprise Technologies, 4 (9 (112)), 23–31. doi: https://doi.org/10.15587/1729-4061.2021.238957